LAWRENCE
LIVERMORE
NATIONAL
LABORATORY

LLNL-TR-704381

Chlorite, Biotite, Illite, Muscovite, and Feldspar Dissolution Kinetics at Variable pH and Temperatures up to 280 °C

S. Carroll, M. Smith, K. Lammers

October 5, 2016

Disclaimer

This work performed under the auspices of the U.S. Department of Energy by Lawrence Livermore National Laboratory under Contract DE-AC52-07NA27344.

Chlorite, Biotite, Illite, Muscovite and Feldspar Dissolution Kinetics at Variable pH and Temperatures up to 280 °C

Susan A. Carroll, Megan M. Smith, and Kristin Lammers
Lawrence Livermore National Laboratory

Summary

Sheet silicates and clays are ubiquitous in geothermal environments. Their dissolution is of interest because this process contributes to scaling reactions along fluid pathways and alteration of fracture surfaces, which could affect reservoir permeability. In order to better predict the geochemical impacts on long-term performance of engineered geothermal systems, we have measured chlorite, biotite, illite, and muscovite dissolution and developed generalized kinetic rate laws that are applicable over an expanded range of solution pH and temperature for each mineral. This report summarizes the rate equations for layered silicates where data were lacking for geothermal systems. Here we report updated rate laws for chlorite (Carroll and Smith 2013), biotite (Carroll and Smith, 2015), illite (Carroll and Smith, 2014), and for muscovite based on data collected FY2016. All rate laws take the following form:

$$R_{diss} = \left[\left(A_{acid} \cdot e^{-E_A/\mathrm{RT}} \cdot a_{\mathrm{H+}}^{n} \right) + \left(A_{neutral} \cdot e^{-E_N/\mathrm{RT}} \right) + \left(A_{basic} \cdot e^{-E_B/\mathrm{RT}} \cdot a_{\mathrm{OH-}}^{m} \right) \right] \cdot f(\Delta G_r) \quad (1)$$

where R_{diss} is a surface area-normalized dissolution rate (mol m^{-2} s^{-1}); A_{acid}, $A_{neutral}$, and A_{basic} (mol m^{-2} s^{-1}) are the apparent pre-exponential rate factors and E_A, E_N, and E_B (kJ mol^{-1}) are the activation energies for the acid, neutral and basic mechanisms that account for temperature dependence; and n and m account for the rate dependence on $H^+_{(aq)}$ and $OH^-_{(aq)}$, respectively. The form of this equation, which includes a reaction affinity term incorporating the Gibbs free energy of reaction, $f(\Delta G_r)$, to slow reaction as equilibrium is approached, can be incorporated into most existing reactive transport codes for use in prediction of rock-water interactions in natural and engineered geothermal systems. For chlorite, illite, and muscovite we used a simple expression of the reaction affinity term derived from transition-state theory, $f(\Delta G_r) = 1 - \exp(\Delta G_r / \mathrm{RT})$.

Combination of new data collected at elevated temperature as well as all available published chlorite, $(Mg,Al,Fe)_{12}(Si,Al)_8O_{20}(OH)_{16}$, dissolution datasets results in a kinetic rate equation that is valid over temperatures of 25-275 °C and 3 ≤ pH ≤ 10:

$$R_{chlorite} = \left(\left[1 \cdot 10^{-4} \cdot e^{-30/\mathrm{R \cdot T}} \cdot a_{H^+}^{0.74} \right] + \left[4.7 \cdot 10^{-11} \cdot e^{-13/\mathrm{R \cdot T}} \right] + \left[1.5 \cdot 10^{-9} \cdot e^{-15/\mathrm{R \cdot T}} \cdot a_{OH^-}^{0.43} \right] \right) \cdot \left(1 - e^{\Delta G_r/\mathrm{RT}} \right)$$

(2)

New data collected at elevated temperature for biotite, $K_2(Mg,Fe,Al)_6(Si,Al)_8O_{20}(OH)_4$, results in a kinetic rate equation that is valid over temperatures of 100-280 °C and 3 ≤ pH ≤ 8.5:

$$R_{biotite} = \left(\left[1.5 \cdot 10^{-4} \cdot e^{-22/\mathrm{R \cdot T}} \cdot a_{H^+}^{1.1} \right] + \left[1 \cdot 10^{-9} \cdot e^{-22/\mathrm{R \cdot T}} \right] \right) \cdot \left(1 - \left[e^{\Delta G_r/RT} \right]^{0.04} \right) \quad (3)$$

Combination of new data collected at elevated temperature as well as all available published illite, $K_{1.8}(Al,Fe,Mg)_4(Si,Al)_8O_{20}(OH)_4$, dissolution datasets results in a kinetic rate equation that is valid over temperatures of 5-280 °C and 2.6 ≤ pH ≤ 9.7:

$$R_{illite} = \left[\left(1\times10^{-2}\cdot e^{-58/RT}\cdot a_H^{0.55}\right)+\left(2\times10^{-5}\cdot e^{-54/RT}\right)+\left(1.5\cdot e^{-77/RT}\cdot a_{OH}^{0.35}\right)\right]\cdot\left(1-e^{\Delta G_r/RT}\right) \quad (4)$$

Combination of new data collected at elevated temperature as well as all available published data for muscovite, $K_2(Mg,Fe,Al)_4(Si,Al)_8O_{20}(OH)_4$, results in a kinetic rate equation that is valid over temperatures of 70-280 °C and 2 ≤ pH ≤ 9.5:

$$R_{muscovite} = \left(\left[3\cdot10^{-3}\cdot e^{-44/R\cdot T}\cdot a_{H^+}^{0.8}\right]+\left[9\cdot10^{-6}\cdot e^{-45/R\cdot T}\right]+\left[5\cdot10^{-11}\cdot e^{-61/R\cdot T}\cdot a_{OH^-}^{0.6}\right]\right)\cdot\left(1-e^{\Delta G_r/RT}\right) \quad (5)$$

The chlorite, biotite, illite, and muscovite rate equations help fill the kinetic data gap for fracture-filling minerals and can be used to assess the impact of geochemical reactions on the sustainability of shear zones for proposed engineered geothermal energy systems (EGS). Reactivity of illite and muscovite are much greater than biotite and chlorite, with as much as 75% of the initial illite mass and 60% of the muscovite mass dissolving over a 3-4 day experiment forming aluminum oxyhydroxides. The extent of illite and muscovite dissolution generally increased with increasing temperature and were less dependent on pH. Net dissolution of chlorite and biotite was minor over the same time period, although the solution chemistry data supports aluminum hydroxides precipitation at acid pH with increasing temperature. Feldspar dissolution rates were measured at 200, 250, and 280C in 6 experiments. No rate law has been developed from this data set.

1.0 Introduction

Development of engineered geothermal energy systems (EGS) through the reactivation of fractures in deep hot rocks requires sustained permeability for about 30 years. Chemical reactions pose an important but poorly understood threat to EGS long-term success, because critical kinetic data necessary to fully assess the risk are lacking for most fracture-filling minerals at EGS target temperatures. The poor understanding of the impact of rock-water interactions on fracture permeability is illustrated by variable results from experimental laboratory studies on fractured rock cores. Some data suggest that chemical reactions can significantly reduce fracture permeability even at temperatures much lower than EGS target zones (200 to 400°C) (Polak et al., 2003; Carlson et al., 2005; Viani et al., 2005; Yasuhara et al., 2006, 2011; Yasuhara and Elsworth, 2008), while others in chemically perturbed environments (e.g., undersaturated or CO_2-rich) show an increase in fracture permeability (Polak et al., 2004; Smith et al., 2013a). It is important to correctly assess the role of chemistry on EGS permeability, because reductions in fracture permeability will negatively affect heat transfer, possibly rendering the EGS system uneconomic. In principle the role of geochemistry could be assessed through modeling. Unfortunately, kinetic data and rate equations are lacking for fracture filling minerals at EGS temperatures (200 to 400°C) and are rare even to 100 °C (Cama et al., 2000; Brandt et al., 2003; Gustaffson & Puidomenech, 2003; Köhler et al., 2003; Carroll and Knauss 2005; Lowson et al., 2005, 2007; Smith et al., 2013b). Use of reaction rates extrapolated from low temperature may overpredict dissolution by up to 10,000 times at typical EGS temperatures, leading to poor estimates of impact of geochemical alteration on EGS permeability (Smith et al., 2013b).

We address this need by measuring dissolution rates and deriving rate equations for fracture minerals identified in shear stimulation zones at EGS demonstration sites. The resulting rate equations can be directly incorporated into larger scale reactive transport simulations to assess the impact of

geochemical reactions on shear zone permeability. In order to better predict the geochemical impacts on long-term performance of engineered geothermal systems, we have measured chlorite, illite, biotite, and muscovite dissolution and developed generalized kinetic rate laws applicable over an expanded range of solution pH and temperature for each mineral. Here we report updated rate laws for chlorite (Carroll and Smith 2013), biotite (Carroll and Smith, 2015), illite (Carroll and Smith, 2014), and for muscovite (Lammers, Smith, and Carroll, 2017).

2.0 Materials & Methods

Chlorite (Mg-rich variety, clinochlore, with trace rutile impurities), identical to that used in previous work (Smith et al., 2013b) and purchased from the Source Clays Repository (Flagstaff Hills "CCa-2" chlorite, El Dorado County, California; described by Post and Plummer, 1972), was used in these experiments. Mineral dissolution rates were calculated from dissolved silica concentrations using the stoichiometry determined by Smith et al. (2013b) of $(Mg_{4.29}Al_{1.48}Fe_{0.10})(Al_{1.22}Si_{2.78})O_{10}(OH)_8$ by electron microprobe and verified with transmission electron microscopy (TEM). The bulk specimen was crushed to pea-size; a reserved portion was then mechanically milled to the 150-250 µm size fraction used in the experiments. Multi-point N_2-BET surface area measurements of the bulk, unreacted micro-mill-ground "CCa-2" chlorite grains provided a value of 4.9 $\pm$0.3 $m^2\ g^{-1}$, similar to the estimate of 5.1 $\pm$0.4 $m^2\ g^{-1}$ for the hand-crushed "CCa-2" chlorite used in Smith et al. (2013b). Chlorite samples reacted in neutral and basic solution pH experiments displayed post-reaction surface area values that were up to three times lower than initial unreacted values. For the purposes of calculating dissolution rates, we use pre-reaction measured surface areas, to remain consistent with rates calculated in previously published chlorite studies. The low iron content and initial surface area differ from values reported for this mineral by the Clay Minerals Society, but have been independently replicated by another research group (Black and Haese, 2014).

A Mg-rich biotite variety (phlogopite) was procured from Dr. Young-Shin Jun (Washington University, St. Louis, USA). Large biotite sheets were shredded in a coffee grinder and then subjected to a 15-sec burst of micro-milling to obtain the 150-250 µm size fraction used in dissolution experiments. No further pretreatment steps were taken. Electron microprobe analysis determined the composition of this mineral as $K_{1.88}(Na_{0.10})(Mg_{5.28},Fe_{0.34},Al_{0.24},Ti_{0.08})(Si_{5.76},Al_{2.24})O_{20}(OH)_{4,}$, and no impurities were noted in XRD or SEM analysis. Initial XRD and TEM analysis confirmed the biotite crystal structure as well as the characteristic 10-Å basal spacing, with no further detection of crystalline impurities. The specific surface area of the 150 – 250 µm unreacted biotite grains was 10.7 $m^2\ g^{-1}$. Solid phases reacted under acidic conditions showed evidence of secondary aluminum oxy-hydroxides (boehmite) in both SEM and XRD, similar to observations from illite and muscovite acid experiments. No indication of secondary precipitates was noted in neutral- or alkaline-reacted solids.

The illite used in our experiments was purchased from the Clay Minerals Society as Special Clay IMt-1 from Silver Hill, Montana, USA. The material was mechanically crushed and sieved to collect the 150-250 µm size fraction. In keeping with previously published experimental work on similar layered silicates (e.g., Sass et al., 1987; Köhler et al., 2003), this size fraction was further treated with an acid wash to remove potential carbonate impurities (Zavarin et al., 2012) before drying and re-sieving. The chemical composition, $K_{1.59}(Na_{0.04},Ca_{0.02})(Al_{2.98},Fe^{III}_{0.47},Fe^{II}_{0.08},Mg_{0.48},Ti_{0.05})(Si_{6.76},Al_{1.23})O_{20}(OH)_4$, was determined by electron microprobe (EMP) and transmission electron microprobe (TEM) analyses. Illite contained some trace amounts of quartz and K-feldspar as detected in both powder diffraction pattern, scanning electron microscopy (SEM), and the TEM analysis. Comparison of XRD patterns for dry and ethylene glycolated samples show that the sample is predominately illite with no indication of expandable smectite clays. The initial surface area of the unreacted 150 – 250 mm size fraction was 34.2 $m^2\ g^{-1}$ as measured by multi-point N_2-BET.

Large flakes of muscovite were obtained from Ward's Scientific. The flakes were mechanically shredded in a coffee grinder and sieved to obtain the 150-250 µm size fraction for use in dissolution experiments but were otherwise used as received. The composition of the muscovite was determined by electron microprobe as $K_{1.74}(Na_{0.21})(Al_{3.87},Fe_{0.17},Mg_{0.02})(Al_{2.01},Si_{5.99})O_{20}(OH)_4$. High-resolution TEM analysis confirmed the 2M1-muscovite crystal structure and characteristic 20 Å spacing. Initial surface areas were 4.23 $m^2\ g^{-1}$ as determined by multi-point N_2-BET. XRD powder analysis detected no significant crystalline impurities in the initial muscovite material.

K-feldspar, from Ward's Scientific, was mechanically ground and sieved to obtain the 150-250 µm size fraction for use in dissolution experiments but were otherwise used as received. The composition was determined by electron microprobe to be 86% K-feldspar, $K_{0.829}Al_{0.926}Na_{0.075}Ti_{0.01}Fe_{.007}Ca_{0.007}Mn_{0.005}Mg_{0.022}Si_{3.00}O_8$ and 14% albite, $K_{0.001}Al_{0.965}Na_{0.489}Ti_{0.01}Fe_{.007}Ca_{0.034}Mn_{0.005}Mg_{0.022}Si_{3.00}O_8$. Initial surface areas were 0.267 $m^2\ g^{-1}$ as determined by multi-point Kr-BET.

All experiments were performed in a background matrix of reagent-grade 0.05m NaCl and distilled deionized water initially purged with N_2 gas to remove atmospheric oxygen. Reagent-grade hydrochloric acid (HCl) and sodium hydroxide (NaOH) were commonly used to adjust the pH of individual solutions to desired levels. Total chloride levels in the experimental solutions were maintained at a constant value of 0.05m, but sodium levels varied up to 0.075m as a result of pH adjustment by sodium hydroxide. Approximately 1g of unreacted chlorite or illite was used for each single temperature/pH flow-through experiments, with smaller quantities (0.4-0.7g) sufficing for biotite and muscovite experiments, and larger masses (~1.5g) used in the stacked illite experiments. Stacked experiments refer to those experiments in which illite dissolution rates were measured at variable temperature (constant pH) using the same solid.

Titanium single-pass mixed-flow reactors (e.g., Dove and Crerar, 1990) were used to conduct dissolution experiments over a temperature range of 100-280 °C and a pH range of 2-10 generally at far-from-equilibrium conditions. A schematic of the experimental set-up is shown in Smith et al. (2013b). Room temperature NaCl solutions were pumped into the experimental reactors to pressurize the system, and then the reactor was brought to temperature over a period of several hours while influent solution continued to flow at a constant flowrate of 0.5 mL min^{-1}. We refer to time t = 0 in Figure 1 as the time when the reactor system achieved its target temperature. Influent solution flowed up over mineral grains held between fine titanium meshes in an isolated sample holder within the experimental reactor, ensuring continuously mixed conditions. Reactor system pressures were maintained well above boiling point pressures by the use of a dome-loaded back-pressure regulator and nitrogen gas at the reactor outlet. All wetted reactor surfaces (including the pump and back-pressure regulator) were made of C-276 alloy, passivated grade-4 titanium, or PEEK. To conclude each experiment, the reactor heaters were turned off and the sample holder was removed from each reactor as soon as liquid temperatures decreased below 100 °C. Sample holders were dried overnight at 60 °C and reacted solids were then removed and preserved for

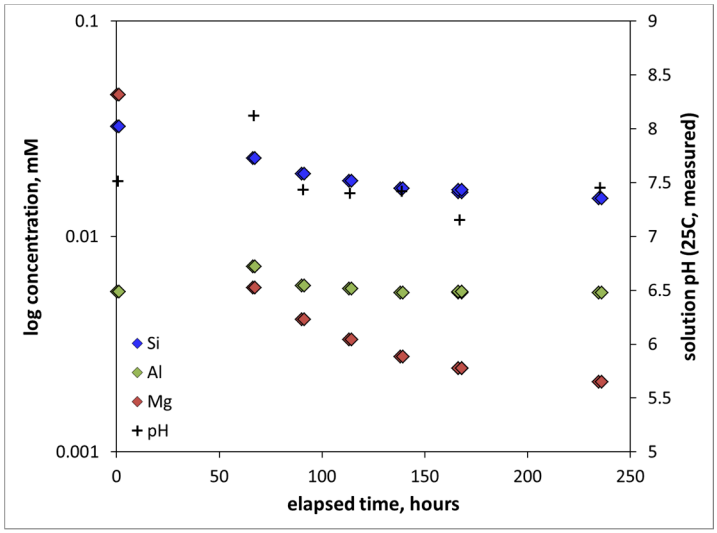

Figure 1: Typical experimental solution chemistry as a function of time. Example is from illite experiment ILS-3 conducted at 100 °C with influent pH 7.4.

post-reaction characterization. Each reactor and pump was cycled with a pH-adjusted cleaning solution followed by at least 24 hours of distilled water rinsing between experiments, and reactor parts were periodically boiled in 8N nitric acid and re-passivated to prevent contamination.

Aqueous samples were collected directly downstream of the back-pressure regulator through a luer-lock port using 60-mL disposable syringes. Effluent samples were split into three aliquots for analysis: 15 mLs were filtered (0.2 um) and acidified for major and trace element analysis (silicon, aluminum, iron, magnesium, potassium, and/or calcium) by inductively-coupled plasma optical emission spectrometry (ICP-OES); 1 mL was filtered and diluted by 10x distilled water for ion chromatography (IC) to confirm consistent background sodium and chloride matrix concentrations and to confirm potassium levels; 3-5 mLs were reserved, unfiltered, for 20 °C pH measurement. The geochemical code EQ3/6 (Wolery, 1992) and the updated *data.ymp* database were used to calculate solution pH at experimental temperatures as well as mineral-specific fluid saturation indices. To avoid propagating large errors from IC measurements into the calculation of solution pH, each solution chemistry dataset was first charge-balanced (on chloride, Cl^-) at 25 °C using measured solution pH values, and then modeled at the experimental temperature for determination of *in situ* solution pH.

3.0 Results & Discussion

In this section we discuss the chlorite, biotite, illite, and muscovite, dissolution rate data and the resulting rate laws. All rate laws take the following form:

$$R_{diss} = \left(\left[A_{acid} \cdot e^{-E_A/_{\mathrm{R}\cdot\mathrm{T}}} \cdot a_{H^+}^{n}\right] + \left[A_{neutral} \cdot e^{-E_N/_{\mathrm{R}\cdot\mathrm{T}}}\right] + \left[A_{basic} \cdot e^{-E_B/_{\mathrm{R}\cdot\mathrm{T}}} \cdot a_{OH^-}^{m}\right]\right) \cdot f(\Delta G_r) \quad (1)$$

where R_{diss} (mol m^{-2} s^{-1}) is a surface area-normalized dissolution rate; A_{acid}, A_{neut}, and A_{basic} (mol $m^{-2}s^{-1}$) are the apparent pre-exponential rate factors and E_A, E_N, and E_B (kJ mol^{-1}) are the activation energies for the acid, neutral and basic mechanisms that account for temperature dependence, and *n* and *m* account for the rate dependence on $H^+_{(aq)}$ and $OH^-_{(aq)}$, respectively. The final term represents some functional dependence of the overall rate on the Gibbs free energy of reaction, ΔG_r, to slow the reaction rate as equilibrium is approached. Nagy and Lasaga (1992) provide an overview of transition state theory (TST) and its application to the affinity term, as well as empirical variants of this term. Most of our experiments were sufficiently far from equilibrium to be affected by an affinity term. For chlorite, illite, and muscovite we used the TST-based term (1-exp(ΔG_r/RT)) because there was no justification for using a more complex form. Specific rate parameters values are included in the mineral-specific rate equations (2-5). It is important to note that the generalized kinetic rate equation yields highly correlated mechanism-specific parameter values (e.g., A_A, E_A, and *n* all strongly correlated; likewise A_B, E_B, and *m*) when fit to the data. Given this non-uniqueness (Smith and Carroll, 2016; Cama et al., 2000) graphical methods or literature values of independently estimating E_i, *n*, and *m* were utilized to reduce the number of unknown model parameters. Final equations were derived by a combination of visual (spreadsheet-based) fitting methods as well as PEST (parameter optimization code, Doherty et al., 2005). The resulting rate equations can be incorporated into most existing reactive transport codes for use in prediction of rock-water interactions in engineered geothermal systems.

3.1 Chlorite

We limit our discussion of chlorite dissolution rates to the derivation of the rate law and key findings. Additional details can be found in Smith et al. (2013b) and Smith and Carroll (2016). The recommended rate equation for chlorite, $(Mg,Al,Fe)_{12}(Si,Al)_8O_{20}(OH)_{16}$, is dependent on both pH and temperature and utilizes three different dissolution mechanisms (acid, neutral, and basic), and was

derived from 100-275 °C rate data collected in these studies as well as available published data from other sources from 25-120 °C (Brandt et al., 2003; Lowson et al., 2005, 2007; Black and Haese, 2014; Zhang et al., 2015). The data and fit to rate equation is shown in Figure 2. Combination of new data collected at elevated temperature as well as all available published chlorite dissolution datasets results in a kinetic rate equation that is valid over temperatures of 25-275 °C and 3 ≤ pH ≤ 10:

$$R_{chl} = \left(\left[1 \cdot 10^{-4} \cdot e^{-30/\mathrm{R \cdot T}} \cdot a_{H^+}^{0.74}\right] + \left[4.7 \cdot 10^{-11} \cdot e^{-13/\mathrm{R \cdot T}}\right] + \left[1.5 \cdot 10^{-9} \cdot e^{-15/\mathrm{R \cdot T}} \cdot a_{OH^-}^{0.43}\right]\right) \cdot \left(1 - e^{\Delta G_r/\mathrm{RT}}\right) \quad (2)$$

These estimated activation energies are relatively low compared to the reported range for layered silicate minerals (~20-90 kJ mol^{-1}) and are 3-4 times lower than previously estimated values for chlorite dissolution (Nagy, 1995; Palandri and Kharaka, 2004), but are consistent with values previously reported by Smith et al. (2013b) and Black and Haese (2014).

Rates with $\Delta G_r \geq$ -65 kJ mole^{-1} (rates *closer* to equilibrium, n = 58) were used to assess the appropriateness of various reaction affinity terms $f(\Delta G_r)$. We find that chlorite dissolution is best described by a reaction affinity term based on transition-state theory, suggesting that the approach to equilibrium should lower the rate only when solutions are very close to equilibrium, i.e., rates with $\Delta G_r \geq$ -2 kJ mol^{-1} (or $SI >$ -0.5, where SI is equal to log IAP/K_{eq}, where IAP is the ion association production and K_{eq} is the equilibrium constant for the mineral of interest).

We find that the dissolution of chlorite, a sheet-silicate, is relatively slow at elevated temperatures (100-275 °C), compared to other framework silicate minerals for which higher-temperature kinetic data are available (e.g., quartz and feldspars; see Palandri and Kharaka, 2004). This finding and the overall variation of only ~2 orders of magnitude difference in rate values measured over 25 to 275 °C, provides the basis for relatively lower activation energies for the specific rate mechanisms, in conflict with previously reported high activation energies for chlorite based on extrapolation of low-temperature experimental data to higher temperatures. Additionally, we note that the dissolution rate of chlorite does not increase in alkaline pH conditions, as has been noted for other minerals, but rather remains at the same level as that noted for neutral conditions, with only a weak dependence on temperature. Despite an additional minimal dependence of the rate on alkaline solutions (non-parabolic rate behavior), we find that a separate alkaline rate mechanism is necessary to prevent rate models from underpredicting rates at high pH. The available rate data at high pH cannot differentiate whether this lack of rate dependence at alkaline pH is due to decreased effects of hydroxide-catalyzed reaction or increased effects of fluid saturation under these conditions.

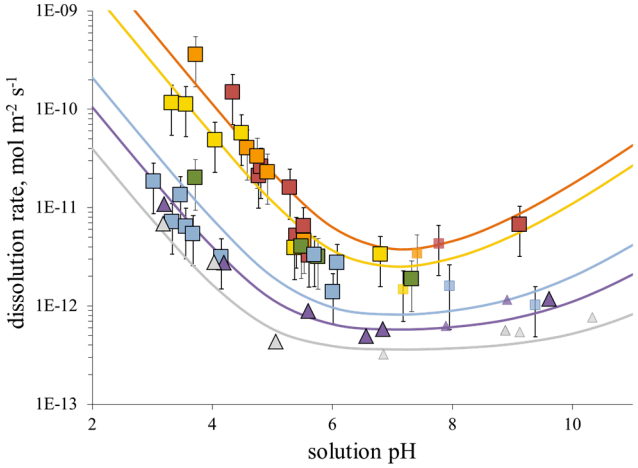

Figure 2: Chlorite dissolution rates versus solution pH, from Smith and Carroll (2016), including data from that work and Smith et al., 2013, (□); and Lowson et al., 2007 (Δ). Solid lines represent fitted rates at corresponding temperatures calculated from 25-275 °C equation (2). Smaller symbols represent rates measured under $\Delta G_r \geq$ -65 kJ mol^{-1} conditions.

3.2 Biotite

Phlogopite, a Mg-rich biotite, $K_2(Mg,Fe,Al)_6(Si,Al)_8O_{20}(OH)_4$, was reacted under elevated temperature conditions at a wide range of pH to investigate its reactivity in comparison to similar K-deficient and Mg,Fe-deficient sheet silicates (chlorite, illite, and muscovite).

Like these other minerals, the stoichiometry of biotite dissolution is highly dependent on solution pH (Figure 3). At acid conditions, silica, magnesium, and potassium are released congruently, but aluminum is detected at much lower levels. As pH increases aluminum and silica release becomes stoichiometric, while magnesium release rates begin to decrease relative to silica and potassium release rates remain consistently (2-3 orders of magnitude) faster than silica rates. These geochemical findings are consistent with SEM observations of Al-rich precipitates (identified as boehmite, γ-AlO(OH), by XRD) on the surface of biotite grains reacted under acidic pH, similar to that noted for illite and muscovite. Given the detection of Al-oxyhydroxide precipitates but no indication of aluminosilicate precipitation, biotite dissolution rates were calculated from dissolved silica levels (Figure 4a).

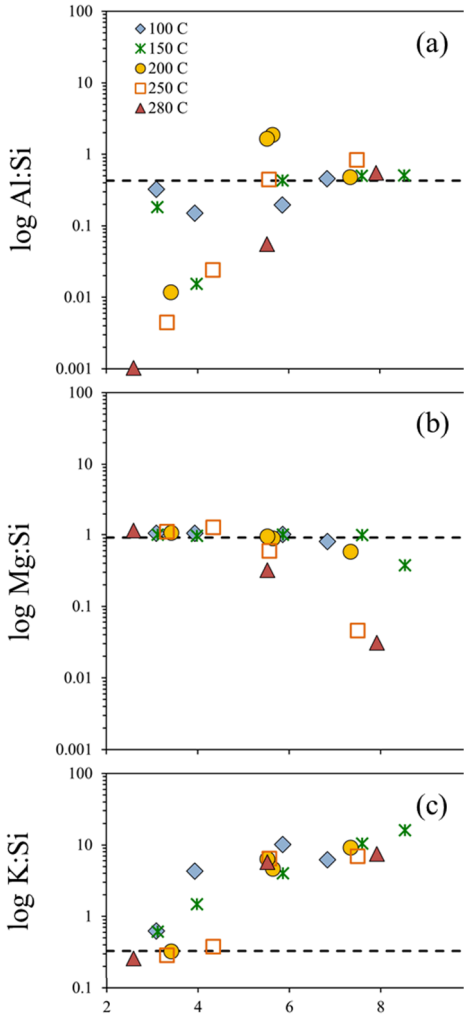

Figure 3: Log ratio of steady-state a) Al:Si, b) Mg:Si, and c) K:Si versus solution pH at temperature from biotite dissolution experiments. Heavy dashed line indicates the ratio present in unreacted biotite.

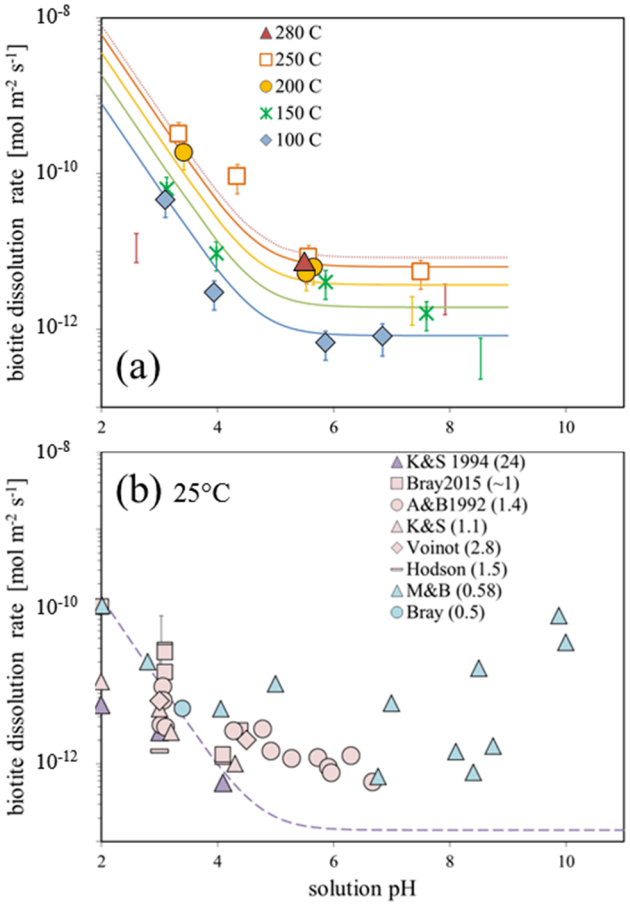

Figure 4: Biotite dissolution rates versus pH from a) this study, 100-280 °C; and b) previously published work at 25 °C. Rate predictions are shown as lines of corresponding color. Rate equation (3) is shown as solid lines in a) and as a single 25 °C dashed line in b). Note that color and number in parentheses in plot b) denote initial biotite Mg:Fe ratio. References: Acker and Bricker, 1992; Kalinowski and Schweda, 1994; Malmstrom and Banwart, 1997; Hodson, 2006; Voinot et al., 2013; Bray et al., 2015.

Enhanced potassium release has been noted by many previous researchers (e.g., Gilkes and Yound, 1974; Kalinowski and Schweda, 1996; Hu and Jun, 2012). While increased K:Si ratios could indicate the co-precipitation of an aluminosilicate phase, none was noted either in this study or the previous cited ones. These higher values could also be linked to enhanced exchange of K^+ for Na^+ ions (supplied by the background NaCl brine composition). Networks of cracks, similar to those noted by Sánchez-Pastor et al. (2010), were observed on grain surfaces from 200 °C experiments over a range of pH, supporting cation exchange.

Like chlorite, biotite dissolution rates are not strongly dependent on temperature, and increase at most by 10 times from 100 to 280 °C. However, the rates are dependent on pH. At all T $\leq$ 250 °C, rates increase with increasing acidity while remaining flat or even decreasing as pH increases above ~6-7. The behavior at alkaline pH is in contrast with the 25 °C rate trends with alkaline pH (e.g., Figure 4b). Both acid and alkaline rates measured at 280 °C (pH 2.6, 7.9, respectively) are far slower than lower-temperature rates at comparable pH; note that these rates and selected others (log IAP/K_{eq} < -5) were not used to derive the far-from-equilibrium biotite dissolution model and are shown only with error bars in Figure 8a.

The rate of biotite dissolution from 100-280 °C can be described as:

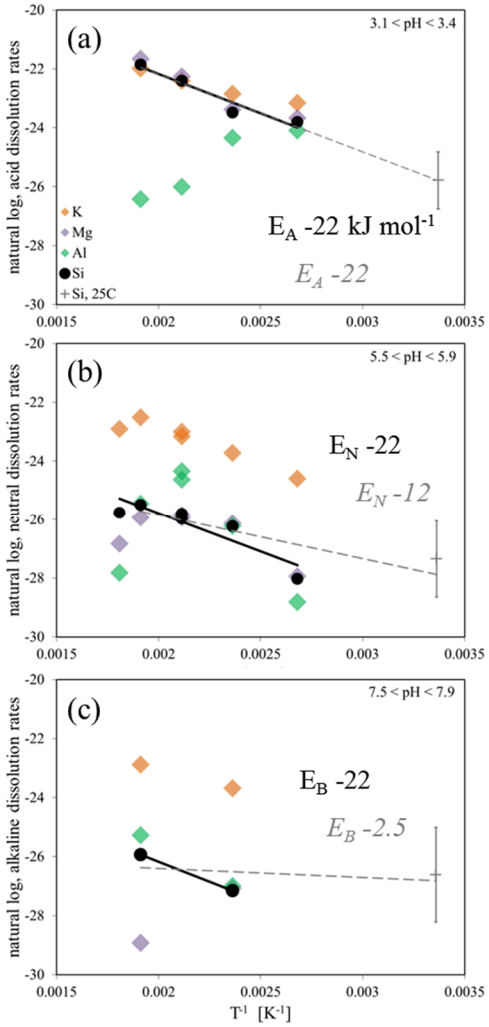

Figure 5: Natural log biotite dissolution rate (mol m^{-2} s^{-1}) versus inverse temperature (K^{-1}) with pH (a-c). K (orange); Al (green); Mg (purple); Si (black); 25 °C literature average (grey cross). Solid bold lines are slopes fitted to data from this study only; grey dashed lines include 25 °C data.

$$R_{biotite} = \left(\left[1.5 \cdot 10^{-4} \cdot e^{-22/\mathrm{R \cdot T}} \cdot a_{H^+}^{1.1}\right] + \left[1 \cdot 10^{-9} \cdot e^{-22/\mathrm{R \cdot T}}\right]\right) \cdot \left(1 - \left[e^{\Delta G_r/RT}\right]^{0.04}\right) \quad (3)$$

Following the protocol of our previous work, we constrain apparent activation energies through use of Arrhenius plots of 100 to 280 °C data, both with and without 25 °C literature rates (Figure 5). If the 100 to 280 °C data from this study is considered alone, a single apparent activation energy value of 22 kJ mol^{-1} is sufficient to describe reaction across acid, neutral, and alkaline pH regimes. The inclusion of 25 °C rate values does not affect the acid value, but decreases the neutral and basic energy values to 12 and 2.5 kJ mol^{-1} respectively. Parameters *n* and *m* = 0.8-0.85 were also fitted graphically (plots not

shown; only a few data points are available to constrain the dependence of the rate on hydroxide activity; *m*).

Graphical and visual fitting to far-from-equilibrium (defined here as log IAP/K_{eq} < -5) from this study (i.e., 100-280 °C) does not require the use of a basic/alkaline pH-mediated mechanism (perhaps due limited number of data). This form of the rate equation fits the majority of the 100-250 °C data well but overestimates the 280 °C rate values at both pH extremes (equation (3); Figure 4a). This rate model also underestimates the 25 °C literature rates for all pH > 5 for from Fe-rich biotite. Biotite with higher Fe:Mg content have rates that are 10 times higher (Kalinowski and Schweda, 1996).

As we have emphasized in previous studies, kinetic rate equations applied to natural systems should incorporate some form of reaction affinity term to slow reaction. While the current biotite dataset would benefit from the addition of targeted near-equilibrium rate data, the apparent "slowing" of some rates at pH extremes allows for testing of selected affinity terms. Our observation is that one 280 °C rate at acid pH (where biotite saturation is not favored) and several rates at pH > 7 (where fluids approach equilibrium with biotite) do not follow the 25 °C trend of increasing rate magnitude with both decreasing and increasing pH. The effect of the affinity term addition will be most pronounced for these rates. The standard TST-based expression was found not to have any effect on predicted rate magnitudes at our modeled saturation indices, but the addition of an exponent, p = 0.04, to generate a nonlinear relationship between saturation index (or Gibbs free energy) allowed rates at higher pH to be dramatically better predicted:

$$f(\Delta G_r) = 1 - \left(\exp\left[\frac{\Delta G_r}{\mathrm{RT}} \right] \right)^p$$

The effect of this affinity term is shown in Figure 6. For those rates already under-predicted by the proposed kinetic model (e.g., at acid pH conditions where ΔG_r values are strongly negative), a further slowing of the predicted rate only slightly worsens the fit of the model to the data, but this same term can drastically improve the fit as fluid saturation indices increase at higher pH.

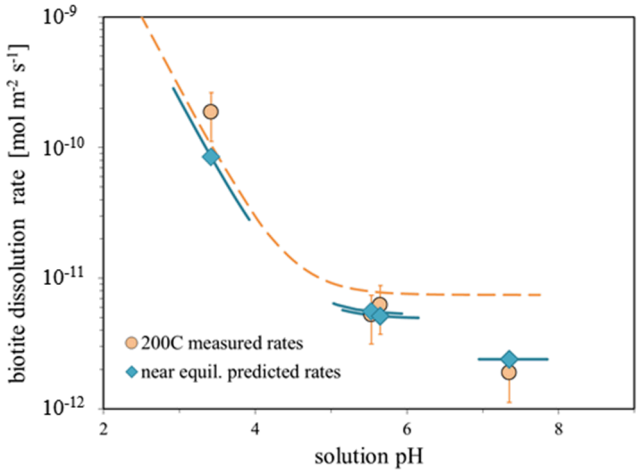

Figure 6: Measured biotite dissolution rates (mol m^{-2} s^{-1}, yellow circles) and predicted FFE rates (yellow dashed line); predicted near-equilibrium (NE) rates (blue diamonds) and NE rate model with p = 0.04 (blue lines). All rates 200 °C, this study.

3.3 Illite

The results of the illite kinetic study are summarized in Smith et al., 2016. Illite, $K_{1.8}(Al,Fe,Mg)_4(Si,Al)_8O_{20}(OH)_4$, is highly reactive at geothermal temperatures, resulting in the precipitation of α/ϒ-AlOOH phases at pH < 5 and 150 to 280°C. The secondary phase sandwiched between illite layers near the grain surface was identified as diaspore (α -AlOOH) with high resolution TEM analysis, whereas the bulk precipitate formed from solution was identified as boehmite (γ-AlOOH) by XRD. No aluminosilicate phases (such as talc or kaolinite) were detected from XRD or TEM analysis. No secondary phases were detected when illite was reacted at neutral or basic pH.

The non-stoichiometric concentrations of K, Al, and Si in the aqueous samples used to measure the dissolution rate are consistent with the detection of Al-oxyhydroxides found in the reacted illite. Figure 7 shows the ratio of steady-state dissolved aluminum and silica concentrations from all illite experiments. Aluminum is highly depleted relative to silica for experiments conducted at pH < 6, as a

result of retrograde aluminum solubility at elevated temperature (Bourcier et al., 1993). Similar observations have been made for feldspar dissolution (Carroll and Knauss, 2005). Over the range of pH 6-8, aluminum to silica ratios approach the value measured in the unreacted illite, and for pH > 8, dissolution appears to proceed roughly stoichiometrically with respect to these two elements. In contrast, ratios of potassium to silica release are largely stoichiometric across the range of pH 3-10 for all temperatures greater than 100 °C. The 100 °C data display increasingly non-stoichiometric K:Si behavior at neutral pH, with values decreasing to that found in the original illite material at 3 > pH > 8. This non-stoichiometric K:Si release at 100 °C is not fully understood. Thermodynamic analysis shows that fluids are undersaturated with respect to illite at this temperature for all pH conditions. The release of K at 100 °C may be due to cation exchange (also observed at 25 °C by Bibi et al., 2011).

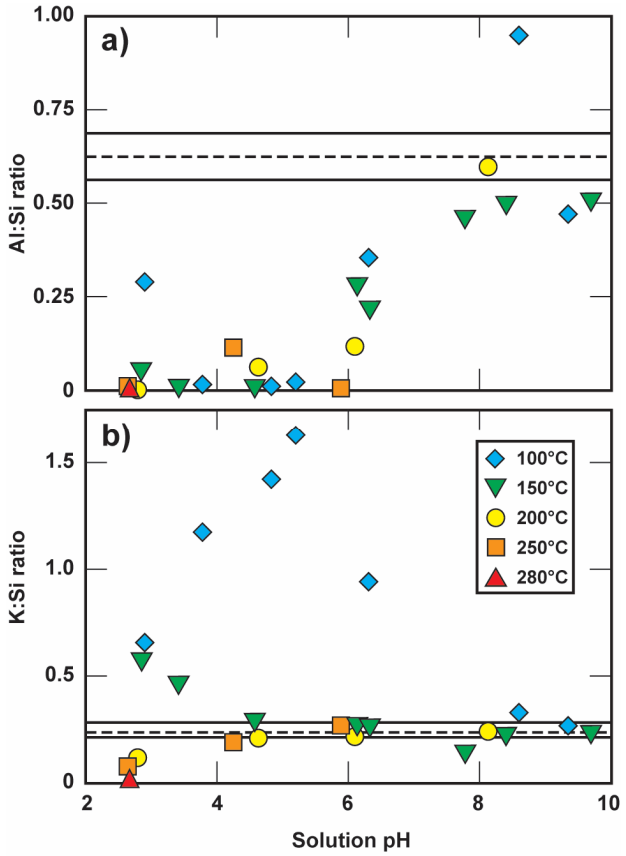

Figure 7: Ratio of steady-state dissolved a) Al:Si, and b) K:Si as a function of pH during illite dissolution. Al:Si and K:Si present in the unreacted illite is represented by the dashed horizontal line, with solid bounding lines representing uncertainty in the original illite ratios as determined by 20+ electron microprobe spot analyses.

Silica concentrations were used to derive the rates shown in Figure 8 because this element best reflects wholesale dissolution of illite, and is not affected by the precipitation of the Al-oxyhydroxide. Dissolved rates were corrected to the final amount of illite in the sample, calculated from integration of each experiment's silica concentration data with time and constant flowrate. Over acid to neutral conditions rates are relatively insensitive to pH, but have a stronger dependence at pH > 7 where the rates increase 0.5-1 orders of magnitude. Rates based on dissolved silica concentrations at 250 and 280 °C fall off the trend established by silica concentrations below 150 °C at pH < 3.5. We attribute these lower values to the extensive dissolution of illite and uncertainty in estimating the final amount of illite and its reactive surface area.

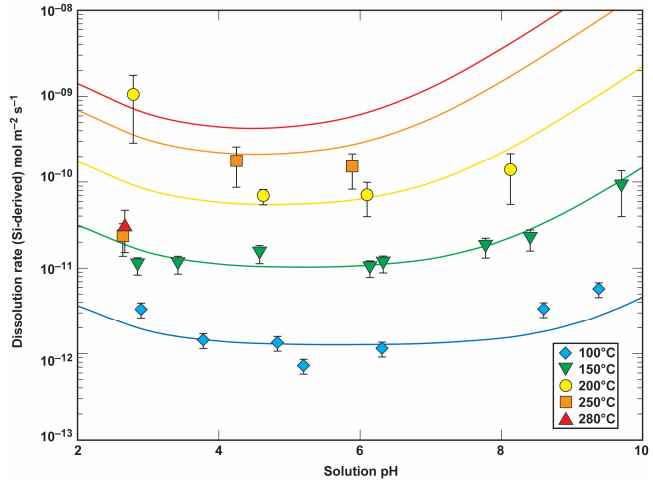

Figure 8: Illite dissolution rates versus solution pH for experiments at temperatures 100-280 °C (this work). Curves indicate rates predicted by equation (3).

Combination of new data collected at elevated temperature in this study as well as all available published illite dissolution datasets from 5 to 50 °C (Bibi et al., 2011; Köhler et al., 2003) results in a kinetic rate equation that is valid over

temperatures of 5-280 °C and 3 ≤ pH ≤ 10, as represented by the solid lines in Figure 8:

$$R_{illite} = \left[\left(1\times10^{-2}\cdot e^{-58/RT}\cdot a_H^{0.55}\right)+\left(2\times10^{-5}\cdot e^{-54/RT}\right)+\left(1.5\cdot e^{-77/RT}\cdot a_{OH}^{0.35}\right)\right]\cdot\left(1-e^{\Delta G_r/RT}\right) \quad (4)$$

Arrhenius plots (natural log of measured rates versus inverse temperature) were used to estimate apparent activation energies over discrete pH intervals to account for the temperature dependence of illite dissolution (Figure 9). Apparent activation energies were derived from best-fit slopes to Si-derived rates from this study and from lower-temperature Si-derived rates collected by Köhler et al. (2003) and Bibi et al. (2011). These values range from ~54-58 KJ mol^{-1} for the acid and neutral mechanisms (Figures 5a-d), up to 77 kJ mol^{-1} for the alkaline/basic mechanism (Figure 9e). Use of these graphically derived apparent activation energies reduced the number of remaining parameters to be fitted in the illite rate equation. Note that these apparent energy values are 10-40 kJ mol^{-1} higher than those arrived at by Köhler et al. (2003) from consideration of 5-50 °C data but are in agreement with respect to relative order, with $E_B > E_A \geq E_N$.A reaction affinity term is necessary to allow kinetic dissolution rates in reactive-transport simulators to decrease as fluid-mineral equilibrium is approached, but the limited available data (including previous literature values) is still too small to permit a detailed comparison of the specific formulation of the affinity term. As currently formulated, this rate model reproduces the majority of observed 100-250 °C illite dissolution rates to within ±0.3 orders of magnitude, but overpredicts lower temperature (25,50 °C) rates in the near-neutral pH regime where illite equilibrium is most strongly favored by up to one order of magnitude (data not shown). The transition state theory (TST)-based form shown above in equation (3) does not significantly affect rate magnitudes until fluid-mineral equilibrium is closely approached (i.e., $\Delta G_r \leq 2$ kJ mol^{-1}). In the absence of more data near equilibrium, we advocate for use of the simple TST form, as was applied for chlorite (Smith and Carroll, 2016).

The rate of secondary AlO(OH)$_{(s)}$ precipitation appears to be much faster than the rate of illite dissolution, because the rates showed little variation with pH (similar to the illite data) and produce a comparable apparent activation energy value to that for acid and neutral illite dissolution (E_{app} ~ 54 kJ mol^{-1}). The AlO(OH)$_{(s)}$ rates are 3-5 orders of magnitude slower than boehmite precipitation rates measured at 100 °C (Bénézeth et al., 2008). The much faster rates suggest that AlO(OH)$_{(s)}$ precipitation could be modeled as an equilibrium

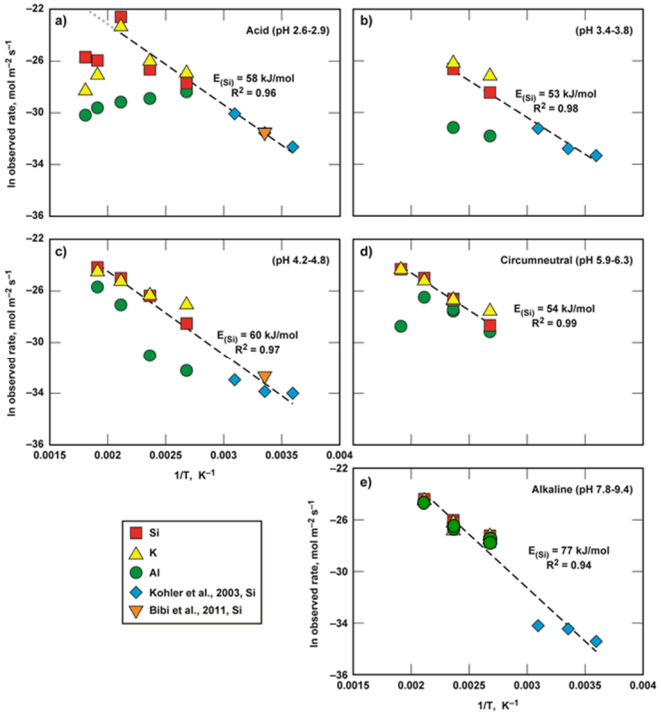

Figure 9: Natural log illite dissolution rates (mol m^{-2} s^{-1}) versus inverse temperature (K^{-1}) with pH (a-e). Element-specific rates from our study are represented by grey squares (Si), green circles (Al), and yellow triangles (K); Si-derived rates from Köhler et al. (2003) and Bibi et al. (2011) are represented as blue diamonds and orange triangles. The Si-derived apparent activation energy derived from the slope of the dashed lines ranges from 54-58 kJ mol^{-1} for pH < 7 (a-d) and 77 kJ mol^{-1} for pH > 7 (e).

process compared to kinetic illite dissolution.

3.4 Muscovite

Muscovite, $K_2(Al,Mg,Fe)_4(Si,Al)_6O_{20}(OH)_4$, is highly reactive at geothermal temperatures, resulting in the precipitation of secondary aluminum oxyhydroxides at pH 4 to 6.5 and 100 to 280 °C. Boehmite (γ-AlOOH) was identified by XRD in acid and higher temperature experiments. No aluminosilicate phases (such as talc or kaolinite) were detected from XRD or TEM analysis.

The non-stoichiometric concentrations of Al:Si in the aqueous samples also supports the precipitation of an Al-oxyhydroxide in experiments where the amount of the secondary precipitate was too small to be detected by XRD. Figure 10 shows the ratio of steady-state dissolved aluminum and silica concentrations from all experiments. Aluminum is highly depleted relative to silica for experiments conducted at pH < 6.5, as a result of retrograde aluminum solubility at elevated temperature (Bourcier et al., 1993; Carroll and Knauss, 2005; see section **3.2**). Over the range of pH 6.5-9.5, aluminum to silica ratios approach but do not reach values measured in the unreacted muscovite. Ratios of potassium to silica release are largely stoichiometric across the range of pH 1.5 to 9.5 for all temperatures greater than 150 °C. The 100 and 150 °C data display non-stoichiometric K:Si behavior at pH < 6 and may be due to cation exchange. All fluids were undersaturated with respect to muscovite.

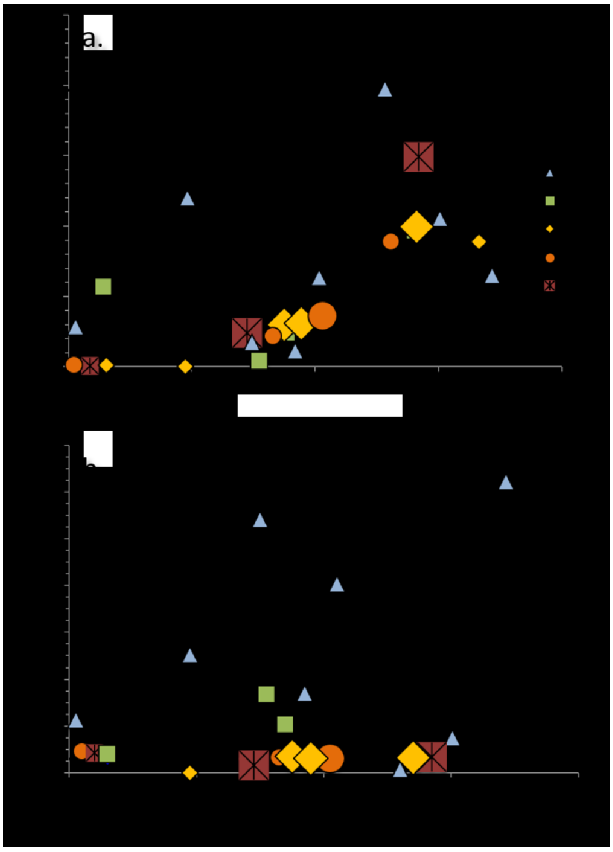

Figure 10. Muscovite dissolution plotted as a) dissolved Al:Si, and b) K:Si as a function of pH. The Al:Si and K:Si in the unreacted muscovite is represented by the dashed horizontal lines.

The dissolution rate of muscovite, $K_2(Al,Mg,Fe)_4(Si,Al)_6O_{20}(OH)_4$,was determined in the same manner as rates for chlorite and illite measuring the rate of silica release reflecting wholesale dissolution. These muscovite dissolution rates versus pH are shown in Figure 11 with data from other studies (Knauss and Wolery, 1989; Oelkers et. al, 2008). The rate equation describes muscovite dissolution over temperatures ranging from 70-280 ˚C and pH 2-9:

$$R_{muscovite} = \left(\left[1 \cdot 10^{-3} \cdot e^{-30/\mathrm{R \cdot T}} \cdot a_{H^+}^{1.0} \right] + \left[9 \cdot 10^{-4} \cdot e^{-62/\mathrm{R \cdot T}} \right] + \left[1 \cdot 10^{-9} \cdot e^{-45/\mathrm{R \cdot T}} \cdot a_{OH^-}^{1.0} \right] \right) \left(1 - e^{\Delta G_r / \mathrm{RT}} \right) \quad (5)$$

Muscovite dissolution rates varied with pH and temperature. The parabolic pH dependence is noticeable for temperature 70˚ C (Knauss and Wolery, 1989), 100 °C (this study) and 150˚C (this study, Oelkers et al., 2008), with slower rates around neutral pH (Figure 12). Measured rates are independent of pH at temperatures ≥ 150 ˚C. Dissolution rates are strongly dependent on temperature increasing by as much as 1,000 times from 70 to 280˚ C.

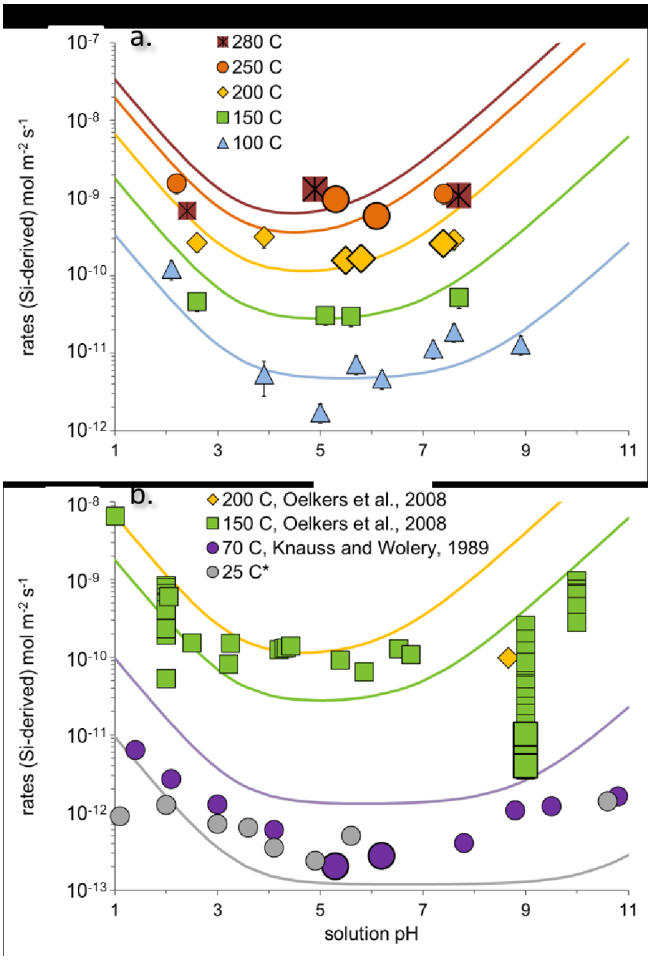

Figure 11: Muscovite dissolution rates versus pH of this study and Knauss & Wolery, 1989, Nickel, 1973 and Oelkers, et al., 2008; predicted by equation (5).

Arrhenius plots of measured rates (natural log) versus inverse temperature (1/K) were used to obtain the activation energies over acidic, neutral and basic regions (not shown). The activation energies for the measured rates are 44 kJ mol^{-1}, 45 kJ mol^{-1} and 61 kJ mol^{-1} for the acid, neutral and basic mechanisms.

3.5 K-Feldspar

K-Feldspar, $KAlSi_3O_8$, dissolution was measured at 200, 250, and 280C for six experiments. No rate equations have been derived for K-Feldspar. Rate data are listed in the Geothermal Data Repository in file *KineticRates_10Feb2017*.

4.0 Conclusions and Implication for Engineered Geothermal Systems

The rate equations summarized in this report should be of use to those who wish to better assess the impacts of geochemical alteration on long-term fracture permeability for EGS systems supported by industry and the Geothermal Program. This is important because geochemical alteration, changing stress fields, mass transport and heat transfer incorporated into computational models are needed to optimize geothermal energy production for EGS systems.

We have measured chlorite, biotite, illite, and muscovite dissolution rates from 100 to 280 °C and pH 2 to 10 to develop comprehensive rate equations that can be used to assess the impact of geochemical reaction on the sustainability of shear zone in natural and/or engineering geothermal reservoirs. The resulting rate equations are dependent on pH, temperature, and reaction affinity and utilize specific dissolution mechanisms (acid, neutral, and basic mechanisms). Rate parameters were derived from data collected at LLNL, and supplemented wherever possible by published rates collected at lower temperatures. The resulting rate equations should be easy to incorporate into most existing reactive transport codes for use in prediction of rock-water interactions in geothermal systems. Data are still lacking for other fracture-filling minerals (epidote, K-feldspar) and for silicate minerals in general at near-equilibrium conditions. The new rate equations are an improvement on extrapolating rates from equations based on low-temperature experiments.

Key findings from the study include

- The rate equations more accurately capture geochemical rates at geothermal conditions than extrapolating available low-temperature equations to higher temperatures.
    - Chlorite rates are up to 10,000 times lower than,

    - Illite and muscovite rates are 10 to 100 times higher than, and
    - Biotite rates are similar to those estimated by extrapolation of low-temperature equations to geothermal temperatures.

- Illite and muscovite are significantly more reactive than chlorite and biotite. Illite and muscovite dissolution increases by about 1000 times from 100 to 280 °C, whereas chlorite and biotite increase by only 10 times over the same temperature range.
- The high reactivity of illite and muscovite is likely to drive chemical alteration in shear zones. Assuming similar abundances and surface areas, reactivity of illite and muscovite are much greater than biotite and chlorite, with as much as 75% of their initial mass dissolving over a 3-4 day experiment. Rapid dissolution and secondary precipitation will likely impact flow and permeability in geothermal reservoirs.

All rate equations and data have been submitted to the Geothermal Data Repository; feldspar rates will be updated as more data becomes available.

Acknowledgements

We acknowledge support of this research through the U.S. Department of Energy, Geothermal Technologies Program. We also wish to thank LLNL personnel Victoria Genetti, Marissa Leever, Rachel Lindvall, Cora Madden, and Josh Wimpenny for solution analysis; Naomi Marks for electron microprobe analysis; and Zurong Dai, Joseph McKeown, and Nick Teslich for microscopy assistance. This work was performed under the auspices of the U.S. Department of Energy by Lawrence Livermore National Laboratory under contract DE-AC52-07NA27344. This report has been reviewed and released under LLNL-TR-704381.

References

Acker J.G., Bricker O.P. 1992. The influence of pH on biotite dissolution and alteration kinetics at low temperature. *Geochimica et Cosmochimica Acta*, 56: 3073-3092.

Bénézeth P., Palmer D.A., Wesolowski D.J. 2008. Dissolution/precipitation kinetics of boehmite and gibbsite: Application of a pH-relaxation technique to study near-equilibrium rates. *Geochimica et Cosmochimica Acta*, 72: 2429-2453.

Bibi I., Singh B., and Silvester E. 2011. Dissolution of illite in saline-acidic solutions at 25 °C. *Geochimica et Cosmochimica Acta* **75**, 3237-3249.

Black J., Haese R.R. 2014. Chlorite dissolution experiments under CO_2 saturated conditions from 50 to 120°C and 120 to 200 bar CO_2. *Geochimica et Cosmochimica Acta*, 125:225-240.

Bourcier W.L., Knauss K.G., Jackson K.J., 1993. Aluminum hydrolysis constants to 2508C from boehmite solubility measurements. *Geochimica et Cosmochimica Acta* 57, 747–762.

Brandt F., Bosbach D., Krawczyk-Bärsch R., Arnold T., Bernhard G. 2003. Chlorite dissolution in the acid pH range: A combined microscopic and macroscopic approach. *Geochimica et Cosmochimica Acta*, 67: 1451-1461. 10.1016/S0016-7037(02)01293-O.

Bray A.W., Oelkers E.H., Bonneville S., Wolff-Boenisch D., Potts N.J., Fones G., Benning L.G. 2015. The effect of pH, grain size, and organic ligands on biotite weathering rates. *Geochimica et Cosmochimica Acta*, 164: 127-145.

Cama J., Ganor J., Ayora C., Lasaga C.A. 2000. Smectite dissolution kinetics at 80°C and pH 8.8. *Geochimica et Cosmochimica Acta*, 64, 2701-2717.

Carlson S.R., Roberts J.J., Detwiler R.L., Viani B.E., Roberts S.K. (2005) Fracture permeability evolution in Desert Peak Quartz Monzonite. *GRC Transactions*, 29, 337-342.

Carroll S.A. and Smith M.M. 2013. Chlorite dissolution kinetics at variable pH and temperatures up to 280°C. Lawrence Livermore National Laboratory, LLNL-TR-644422

Carroll S.A. and Smith M.M. 2014. Illite dissolution kinetics at variable pH and temperatures up to 280°C. Lawrence Livermore National Laboratory, LLNL-TR-663071

Carroll S.A. and Knauss, K. G. 2005. Dependence of labradorite dissolution kinetics on CO_2(aq), Al(aq), and temperature. *Chemical Geology*, **217**, 213-225

Doherty J. 2005. PEST: Software for model-independent parameter estimation. Watermark Numerical Computing, Australia. Available from *http://www.sspa.com/pest; http://www.pesthomepage.org*.

Dove P.M., Crerar D.A. 1990. Kinetics of quartz dissolution in electrolyte solutions using a hydrothermal mixed flow reactor. *Geochim et Cosmochim Acta*, 54:955-969. 10.1016/0016-7037(90)90431-J.

Gustaffson A.B., Puigdomenech I.. 2003. The effect of pH on chlorite dissolution rates at 25 °C. *Materials Res Soc Symp Proc*, 757:649-655. 10.1557/PROC-757-II3.16

Hodson M.E. 2006. Does reactive surface area depend on grain size? Results at 25 °C far-from equilibrium flow-through dissolution experiments on anorthite and biotite. *Geochimica et Cosmochimica Acta*, 70, 1655-1667.

Kalinowski B.E., Schweda P. 1996. Kinetics of muscovite, phlogopite, and biotite dissolution and alteration at pH 1-4, room temperature. *Geochimica et Cosmochimica Acta*, 60, 367-385.

Köhler S.J., Dufaud F., Oelkers E.H. 2003. An experimental study of illite dissolution kinetics as a function of pH from 1.4 to 12.4 and temperature from 5 to 50°C. *Geochimica et Cosmochimica Acta*, 67, 3583-3594.

Knauss K.G.; Wolery, T.J. 1989. Muscovite dissolution kinetics as a function of pH and time at 70˚C. *Geochimica et Cosmochimica Acta*, 53, 1493-1501.

Lammers, K., Smith, M. M., Carroll, S. A. (2017) Muscovite dissolution kinetics as a function of pH at elevated temperature, Chemical Geology (submitted).

Lin F., Clemency C.V. 1981. Dissolution kinetics of phlogopite. I. Closed system. *Clays and Clay Minerals*, 29, 101-106.

Lowson R.T., Comarmond M-C.J., Rajaratnam G., Brown P.L.. 2005. The kinetics of the dissolution of chlorite as a function of pH and at 25°C. *Geochim et Cosmochim Acta*, 69:1687-1699. 10.1016/j.gca.2004.09.028.

Lowson R.T., Brown P.L., Comarmond M-C.J., Rajaratnam G.. 2007. The kinetics of chlorite dissolution. *Geochim et Cosmochim Acta*, 71:1431-1447. 10.1016/j.gca.2006.12.008.

Malmström M., Banwart S. 1997. Biotite dissolution at 25 C: The pH dependence of dissolution rate and stoichiometry. *Geochimica et Cosmochimica Acta*, 61, 2779-2799.

Nagy K.L., Lasaga A.C. 1992. Dissolution and precipitation kinetics of gibbsite at 80 °C and pH 3: The dependence on solution saturation state. *Geochimica et Cosmochimica Acta*, 56, 3093-3111.

Nagy K.L. 1995. Dissolution and precipitation kinetics of sheet silicates, chapter 5, in Chemical Weather Rates of Silicate Minerals, *Reviews in Mineralogy* v31, Eds White A.F., Brantley S.L. Mineralogical Society of America, Washington D.C.

Oelkers, E. H., Schott, J., Gauthier, J-M., Herrero-Roncal, T.H. 2008. An experimental study of the

dissolution mechanism and rates of muscovite. *Geochimica et Cosmochimica Acta*, 72, 4948-4961.

Palandri J., Kharaka Y.K. 2004. A compilation of rate parameters of water-mineral interaction kinetics for application to geochemical modeling. U.S. Geological Survey Open File Report 2004-1068 (70pp).

Polak A., Elsworth D., Yasuhara H., Grader A.S., Halleck P.M. 2003. Permeability reduction of a natural reaction under net dissolution by hydrothermal fluids. *Geophysical Research Letters*, 30, 2020, doi:10.1029/2003GL017575.

Polak A., Elsworth D., Liu J., Grader A.S. 2004. Spontaneous switching of permeability changes in a limestone fracture with net dissolution. *Water Resources Research*, 40, W03502, doi:10.1029/2003WR002717.

Post J.L., Plummer C.C. 1972. The chlorite series of Flagstaff Hill area, California: A preliminary investigation. *Clays and Clay Minerals*, 20, 271-283.

Sánchez-Pastor N., Aldushin K., Jordan G., Schmahl W. 2010. K+-N+ exchange in phlogopite on the scale of a single layer. *Geochimica et Cosmochimica Acta*, 74, 1954-1962.

Sass B.M., Rosenberg P.E., Kittrick J.A. 1987. The stability of illite/smectite during diagenesis: An experimental study. *Geochimica et Cosmochimica Acta*, 51, 2103-2115.

Shao H., Ray J.R., Jun Y-S. 2010. Dissolution and precipitation of clay minerals under geologic CO_2 sequestration conditions: CO_2-brine-phlogopite interactions. *Environmental Science and Technology*, 44, 5999-6005.

Smith M.M., Walsh S.D.C., McNab W.W., Carroll S.A. 2013a. Experimental investigation of brine-CO_2 flow through a natural fracture: Permeability increases with concurrent dissolution/reprecipitation reactions. Proceedings, 38th Workshop on Geothermal Reservoir Engineering, Stanford University, Stanford, CA (February 11-13, 2013).

Smith M.M., Wolery T.J., Carroll S.A. 2013b. Kinetics of chlorite dissolution at elevated temperatures and CO_2 conditions. *Chemical Geology*, 347:1-8. 10.1016/jchemgeo.2013.02.017.

Smith M.M., Carroll S.A. 2016. Chlorite dissolution kinetics at pH 3-10 and temperatures to 275 °C. *Chemical Geology* , 421, 55-64. 10/1016/j.chemgeo.2015.11.022.

Smith M.M., Dai Z., Carroll S.A. 2016. Illite dissolution kinetics from 100 to 280 °C and pH 3 to 9. *Geochimica et Cosmochimica Acta* (in revision).

Smith M.M., Carroll S.A. (2016) Biotite dissolution kinetics at temperatures of 100-280 °C. *Geochimica et Cosmochimica Acta* (in review).

Taylor A.S., Blum J.D., Lasaga A.C., MacInnis I.N. 2000. Kinetics of dissolution and Sr release during biotite and phlogopite weathering. *Geochimica et Cosmochimica Acta*, 64, 1191-1208.

Viani B.E., Roberts J.J., Detwiler R.L., Roberts S.K., Carlson S.R. 2005. Simulating injectate/rock chemical interaction in fracture Desert Peak Quartz Monzonite. *GRC Transactions*, 29, 425-430.

Voinot A., Lemarchand D., Collignon C., Granet M., Chabaux F., Turpault M.-P. 2013. Experimental dissolution vs. transformation of micas under acidic soil conditions: Clues from boron isotopes. *Geochimica et Cosmochimica Acta*, 117, 144-160.

Wolery T.J. 1992. EQ3/6, a software package for geochemical modeling of aqueous systems. Lawrence Livermore National Laboratory Report UCRL MA-110662-PT-1.

Yasuhara H., Polak A., Mitani Y., Grader A.S., Halleck P.M., Elsworth D. 2006. Evolution of fracture permeability through fluid-rock reaction under hydrothermal conditions. *Earth and Planetary Science Letters*, 244, 186-2000.

Yasuhara H., Kinoshita N, Ohfuji H., Lee D S, Nakashima S, Kishida K 2011. Temporal alteration of fracture permeability in granite under hydrothermal conditions and its interpretation by coupled chemo-mechanical model. *Applied Geochemistry*, 26, 2074-2088.

Yasuhara H., Elsworth D. 2008. Compaction of a rock fracture moderated by competing roles of stress corrosion and pressure solution. *Pure and Applied Geophysics*, 165, 1289-1306

Zavarin M., Powell B.A., Bourbin M., Zhao P., Kersting A.B. 2012. Np(V) and Pu(V) ion exchange and surface-mediated reduction mechanisms on montmorillonite. *Environmental Science and Technology*, 46, 2692-2698.

Zhang S., Yang L., DePaolo D.J., Steefel C.I. 2015. Chemical affinity and pH effects on chlorite dissolution kinetics under geological CO2 sequestration related conditions. *Chemical Geology*, 396, 208-217.